Photoinduced nonadiabatic dynamics of ethene: Six-dimensional wave packet propagations using two different approximations of the kinetic energy operator

ARTICLE *in* CHEMICAL PHYSICS · SEPTEMBER 2007

Impact Factor: 1.65 · DOI: 10.1016/j.chemphys.2007.04.002

4 AUTHORS, INCLUDING:

Fabien Gatti
Institut Charles Gerhardt
137 PUBLICATIONS **2,168** CITATIONS
SEE PROFILE

Hans-Dieter Meyer
Universität Heidelberg
245 PUBLICATIONS **9,849** CITATIONS
SEE PROFILE

Available online at www.sciencedirect.com
ScienceDirect
Chemical Physics 338 (2007) 186–199
Chemical Physics
www.elsevier.com/locate/chemphys

Photoinduced nonadiabatic dynamics of ethene: Six-dimensional wave packet propagations using two different approximations of the kinetic energy operator

Michael R. Brill [a,*], Fabien Gatti [b], David Lauvergnat [c], Hans-Dieter Meyer [a]

[a] Theoretische Chemie, Ruprecht-Karls-Universität, Im Neuenheimer Feld 229, D-69120 Heidelberg, Germany
[b] CTMM, Institut Gerhardt (UMR 5253), CC 014, Université Montpellier II, F-34095 Montpellier Cedex 05, France
[c] CNRS, Laboratoire de Chimie Physique (UMR 8000), Université Paris-Sud, F-91405 Orsay, France

Received 19 February 2007; accepted 3 April 2007
Available online 7 April 2007

Abstract

The nonadiabatic dynamics of ethene in its N, V and Z valence states is reinvestigated. Wave packet dynamics initiated by a vertical $\pi \rightarrow \pi^*$ excitation is studied and particular emphasis is put on the investigation of the evolution of diabatic and adiabatic state populations. A new algorithm for computing the adiabatic state populations from diabatically represented wavefunctions is discussed and applied here for the first time. We have used the potential model of ethene which was derived by Krawczyk et al. [R.P. Krawczyk, A. Viel, U. Manthe, W. Domcke, Photoinduced dynamics of the valence states of ethene: a six-dimensional potential-energy surface of three electronic states with several conical intersections. *J. Chem. Phys.* **119** (2003) 1397–1411] and the kinetic energy operator derived by Viel et al. [A. Viel, R.P. Krawczyk, U. Manthe, W. Domcke, Photoinduced dynamics of ethene in the N, V and Z valence states: a six-dimensional nonadiabatic quantum dynamics investigation, *J. Chem. Phys.* **120** (2004) 11000–11010]. However, a second kinetic energy operator, which is more accurate than the first one, was derived and applied. The results of our calculations are in qualitative agreement with the previous ones of Viel et al., but there are marked quantitative differences.

Keywords: Ethene; Nonadiabatic transitions; MCTDH; Wavepacket dynamics

1. Introduction

The $\pi \rightarrow \pi^*$ excitation of a C–C double bond is one of the most fundamental processes in photochemistry and the ethene molecule, which is the smallest hydrocarbon with a C–C double bond, has thus attracted much research, both on its electronic structure [1–8] and on its dynamics [9–13].

In a recent paper, Krawczyk et al. [7] have computed the three lowest potential energy surfaces (PES) of ethene on a CASSCF/CASPT2 level. The three electronic states are denoted as N (normal, π^2), V (valence, $\pi\pi^*$) and Z (zwitterionic, π^{*2}). The geometric configuration of the ethene molecule is described by 12 internal coordinates. However, to make the investigation feasible, the authors considered only the six most important modes, which are torsion, C–C stretching, left and right scissoring and left and right wagging (pyramidalization). The left and right rockings and the four C–H stretches were ignored and their coordinates were fixed to their equilibrium positions. The PES were transformed to a diabatic representation and dynamical calculations were performed by Viel et al. [12] using the multi-configuration time-dependent Hartree (MCTDH) method. The absorption spectrum and in particular the diabatic and adiabatic state populations were discussed.

* Corresponding author. Tel.: +49 6221 545215; fax: +49 6221 545221.
E-mail addresses: michael.brill@pci.uni-heidelberg.de (M.R. Brill), gatti@univ-montp2.fr (F. Gatti), david.lauvergnat@lcp.u-psud.fr (D. Lauvergnat), hans-dieter.meyer@pci.uni-heidelberg.de (H.-D. Meyer).

0301-0104/$ - see front matter © 2007 Elsevier B.V. All rights reserved.
doi:10.1016/j.chemphys.2007.04.002

In the present paper we reconsider this problem using the PES of Krawczyk et al. [7]. We did so for three reasons. Firstly, the MCTDH calculations of Viel et al. [12] were not fully converged, due to the size of the problem and its complicated dynamics. The Heidelberg MCTDH code [14], which we are using, allows for mode-combination and a multi-set description of the electronic states. These features make it much easier to achieve a high convergence (see below). Moreover, the new calculations are performed for a longer propagation time (250 fs rather than 50 or 100 fs). Secondly, Viel et al. [12] used an approximate form of the kinetic energy operator. E.g. all terms which are of order m_H/m_C were neglected. In the present paper we derive and apply a much more accurate – albeit still approximate – form of the kinetic energy operator. And last but not least we want to discuss and apply a new algorithm for computing adiabatic state populations from diabatic wavefunctions.

2. Ethene model and numerical techniques

2.1. Potential energy

The present work is based on the previous publications of Krawczyk et al. [7] and Viel et al. [12]. The potential operator developed there is a three-state diabatic potential matrix which depends on six of the 12 internal coordinates. The degrees of freedom considered are:

- φ, the torsional angle;
- r, the C–C distance;
- α_r, the right scissor angle;
- α_l, the left scissor angle;
- ϑ_r, the right pyramidalization angle;
- ϑ_l, the left pyramidalization angle.

The left and right rocking angle and the four C–H distances were fixed at their equilibrium position.

The three diabatic electronic states are denoted as

- The ground state (N, π^2);
- the valance state, where one π-electron of the C–C double bond is excited (V, $\pi\pi^*$) and
- the zwitterionic state, where both π-electrons are excited (Z, π^{*2}).

whereas the three adiabatic states are denoted as S_0, S_1 and S_2.

An analytic expression for the potential energy operator was obtained by two-body expansions including the six mentioned internal nuclear coordinates. The expansion coefficients have been determined by least-squares fits to CASPT2 *ab initio* data. For more details see Ref. [7].

2.2. The first kinetic energy operator

For the calculation of the kinetic energy operator (KEO) two different approaches were used. The first one, introduced by Viel et al. [12], describes the molecule in a fixed orientation and with six degrees of freedom frozen. To obtain this operator first the 6×6 matrix

$$G^{-1}_{q_i q_j} = \sum_{n=1}^{18} \frac{\partial X_n}{\partial q_i}\frac{\partial X_n}{\partial q_j} m_n \tag{1}$$

has been computed analytically where the X_n are the Cartesian coordinates of the nuclei, the q_i are the six internal degrees of freedom considered and m_n is the mass of the nuclei which belongs to the Cartesian coordinate X_n. Inversion of G^{-1} leads to the G-matrix in terms of which the operator of the kinetic energy reads

$$\widehat{T} = \frac{1}{2}\sum_{i,j=1}^{6} \hat{p}_i^{\dagger} G_{ij} \hat{p}_j \tag{2}$$

Note that by construction this KEO is for a molecule fixed in space (i.e. fixed Euler angles). The KEO for total $J = 0$ contains some additional terms.

Unfortunately the resulting operator is unsuitable for the MCTDH propagation, because it cannot be factorised as a sum of products of one-dimensional operators. Thus two simplifications have been made, (i), neglecting all terms proportional to m_H/m_C and, (ii), restricting the matrix element $G_{\varphi\varphi}$ to its equilibrium value $G_{\varphi,\varphi}(\alpha_0)$ (see Table 1, $\alpha_0 = \angle$HCH). The final expression for the KEO reads

$$\begin{aligned}\widehat{T} = &-\frac{1}{m_h R_{ch}^2}\frac{1}{2\sin^2\left(\frac{\alpha_0}{2}\right)}\frac{\partial^2}{\partial\varphi^2} - \frac{1}{m_C}\frac{\partial^2}{\partial r^2}\\ &-\frac{1}{4m_h R_{ch}^2\left(\cos\left(\frac{\alpha_r}{2}\right)\right)^2}\frac{\partial^2}{\partial\vartheta_r^2} - \frac{1}{4m_h R_{ch}^2\left(\cos\left(\frac{\alpha_l}{2}\right)\right)^2}\frac{\partial^2}{\partial\vartheta_l^2}\\ &-\frac{1}{m_h R_{ch}^2}\frac{1}{\sqrt{\cos\left(\frac{\alpha_r}{2}\right)}}\frac{\partial}{\partial\alpha_r}\cos\left(\frac{\alpha_r}{2}\right)\frac{\partial}{\partial\alpha_r}\frac{1}{\sqrt{\cos\left(\frac{\alpha_r}{2}\right)}}\\ &-\frac{1}{m_h R_{ch}^2}\frac{1}{\sqrt{\cos\left(\frac{\alpha_l}{2}\right)}}\frac{\partial}{\partial\alpha_l}\cos\left(\frac{\alpha_l}{2}\right)\frac{\partial}{\partial\alpha_l}\frac{1}{\sqrt{\cos\left(\frac{\alpha_l}{2}\right)}}\end{aligned} \tag{3}$$

For more details see Ref. [15].

2.3. The second kinetic energy operator

The polyspherical approach Refs. [16–21] is a very successful method for deriving kinetic energy operators. The formalism, which is based on a polyspherical parameterization of an N-atom system, is very general and can be applied whatever the number of atoms and whatever the set of vectors: Jacobi, Radau, valence, satellite, etc. The

Table 1
Equilibrium geometry of ethene. The molecule is planar and of D_{2h} symmetry, i.e. the torsion, rocking and wagging angles vanish at equilibrium

r(C–C) = 1.3321Å
r(C–H) = 1.0806Å
∠HCH = 117.284°

operator is not restricted to the total $J = 0$ case and hence may include overall rotation and Coriolis coupling, although in the following we will assume $J = 0$ exclusively.

The polyspherical approach begins with choosing a set of $N - 1$ vectors which connect the N atoms of the system. For the present case the five vectors, $\vec{R}_i$ ($i = 1, \ldots, 5$), which are depicted in Fig. 1, are chosen to parameterize the configuration of C_2H_4. $\vec{R}_5$ is the vector joining the two C-atoms, $\vec{R}_4$ and $\vec{R}_3$ are the vectors joining the H-atoms, and $\vec{R}_2$ and $\vec{R}_1$ are the vectors joining the C-atoms to the centers of mass of the H_2 subsystems (GH_2). These five vectors are in turn parameterized by 12 polyspherical coordinates (R_1, R_2, R_3, R_4, R_5, θ_1, θ_2, θ_3, θ_4, φ_1, φ_2, φ_3), and three Euler angles which orient the molecule such that $\overrightarrow{R_5}$ is parallel to the body-fixed z-axis and $\overrightarrow{R_4}$ lies in the (xz, $x > 0$) body-fixed half-plane. All the vectors $\vec{R}_1$, $\vec{R}_2$, $\vec{R}_3$, $\vec{R}_4$ are parameterized by their spherical angles in the body-fixed frame: the angles θ_i are explicitly depicted in Fig. 1, the angles φ_i are the dihedral angles ($\varphi_4 = 0$ since $\vec{R}_4$ is in the body-fixed xz plane). In particular, φ_3 is the torsional angle as defined in Ref. [12], i.e. the angle between the two vectors connecting the hydrogen atoms of the CH_2 subsystems (here $\overrightarrow{R_3}$ and $\overrightarrow{R_4}$). The particular choice of the vectors is motivated by the attempt to arrive at coordinates which are as close as possible to the ones used by Viel et al. [12].

The 12D kinetic energy operator of the C_2H_4 molecule in polyspherical coordinates appears as a particular case of the general expression which is discussed in Ref. [19] and reviewed recently in Ref. [20]. Comparing with Eq. (4) and (A1) of Ref. [19] one has to apply these general equations to the present case characterized by $N = 6$ atoms and a vanishing total angular momentum, $J = 0$. The algorithm, outlined in Ref. [19], yields the KEO

$$\widehat{T} = \frac{1}{2}\sum_{n,m=1}^{12} \hat{p}_n^{\dagger} G_{nm} \hat{p}_m \tag{4}$$

where $\hat{p}_n$ denote the momenta conjugate to the 12 polyspherical coordinates.

As always within the polyspherical approach [19], this operator can be written as a sum of products of monomode

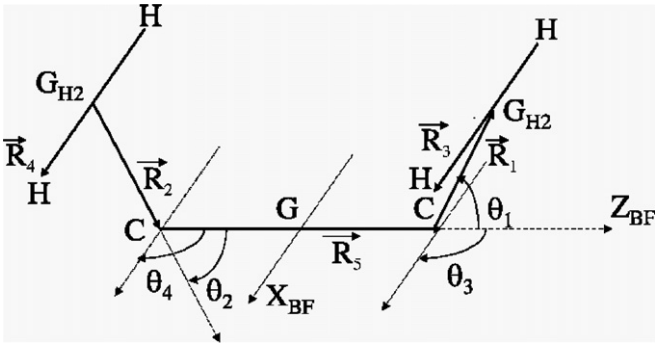

Fig. 1. Polyspherical coordinates for C_2H_4. G is the center of mass of the system. GH_2 denotes the center of mass of the H_2 subsystem.

operators. This property is very profitable for MCTDH. The full 12D operator is not given here since we did not use it.

Indeed, since the potential energy surface is given only in terms of six degrees of freedom, we subject the system to the following constraints:

$$\theta_3 = \frac{\pi}{2}$$
$$\theta_4 = \frac{\pi}{2}$$
$$\varphi_2 = \frac{\pi}{2}$$
$$\varphi_1 = \frac{3\pi}{2} + \varphi_3$$
$$R_3 = 2\sqrt{R_{\mathrm{CH}}^2 - R_1^2}$$
$$R_4 = 2\sqrt{R_{\mathrm{CH}}^2 - R_2^2}$$

where R_{CH} denotes the equilibrium C–H distance. After a simple change of coordinates, the transformation for φ_1, R_3, and R_4 can be expressed by a rigid constraint.

Consequently, we have to deal with a constrained operator which cannot be directly obtained from Eq. (4). In Refs. [21,22], the rigorous derivation of rigidly and adiabatically constrained kinetic energy operators was presented in a full *ab initio* and general context (see also Refs. [23,24]). The method is as follows. In the rigidly or adiabatically constrained approaches, certain internal degrees of freedom, the m inactive coordinates $\mathbf{q}''$, are frozen or adjusted to those of other degrees of freedom, the $n = 3N - 6 - m$ active coordinates $\mathbf{q}'$. The constraint-free kinetic energy operator reads

$$2\widehat{T} = \left[\widehat{\mathbf{P}}'^{\dagger}\widehat{\mathbf{P}}''^{\dagger}\right]\begin{bmatrix}\mathbf{G}' & \boldsymbol{\sigma}^{\mathrm{T}} \\ \boldsymbol{\sigma} & \mathbf{G}''\end{bmatrix}\begin{bmatrix}\widehat{\mathbf{P}}' \\ \widehat{\mathbf{P}}''\end{bmatrix} \tag{5}$$

where the sandwiched matrix is the full $(3N - 6)$-dimensional G-matrix.

If the inactive coordinates are fixed once and for all, the $m = 3N - 6 - n$ rigid constraints can be expressed as

$$q_i'' = q_i''|_0, \quad i = 1, \ldots, m \tag{6}$$

The resulting rigorous kinetic energy operator can be obtained by subjecting the system to the coordinate transformation from $\{q', q''\}$ to $\{q', q''|_0\}$. We then obtain the following expression of the constrained kinetic energy operator [21,22]:

$$2\widehat{T}_{\mathrm{rigid}} = \widehat{\mathbf{P}}'^{\dagger}(\mathbf{G}' - \boldsymbol{\sigma}^{T}\mathbf{G}''^{-1}\boldsymbol{\sigma})|_0\widehat{\mathbf{P}}' \tag{7}$$

where '$(|_0)$' means that the inactive coordinates are fixed to their equilibrium geometry.

It should be noted that another correction due to Eq. (6b) in Ref. [22] must be added, if the Jacobian of the transformation from $\{q', q''\}$ to $\{q', q''|_0\}$ depends on the active coordinates. Usually this correction leads to an extra-potential term (see equation (8) in Ref. [22]).

The constrained operator in Eq. (7) is a sum of two terms. The first term, called the main term, reads

$$T_{\text{main}} = \frac{1}{2}\hat{\mathbf{P}}'^{\dagger}\mathbf{G}'|_0\hat{\mathbf{P}}' \tag{8}$$

It can be directly obtained from the operator without constraints (Eq. (4)) simply by removing all terms involving conjugate momenta associated with the inactive coordinates, P''. If polyspherical coordinates are used, this term can always be written as a sum of products of monomode operators and can be directly obtained from Eq. (4) and is given in Eq. (11) below for C_2H_4.

The second term

$$T_{\text{cor}} = -\frac{1}{2}\hat{\mathbf{P}}'^{\dagger}(\boldsymbol{\sigma}^{\mathrm{T}}\mathbf{G}''^{-1}\boldsymbol{\sigma})|_0\hat{\mathbf{P}}' \tag{9}$$

is a correction. If there is no coupling (in the operator without constraints, Eq. (5)) between the active coordinates and the inactive coordinates, this term vanishes. In general, this correction is numerically smaller than the main term but can play a non-negligible role in the dynamics (see for instance [25] for a discussion on the importance of this term). Unfortunately, the analytical expression of this operator can be very involved and, above all, this correction even when using polyspherical coordinates cannot be written as a sum of products of monomode operators, because the inverse of the matrix G'' will in general depend on the coordinates in a complicated non-separable way. This problem can be removed by introducing an additional reasonable approximation. We fix $(-\boldsymbol{\sigma}^{\mathrm{T}}\mathbf{G}''^{-1}\boldsymbol{\sigma})|_0$ to its value at the equilibrium geometry. The approximated correction thus reads

$$T_{\text{cor}'} = -\frac{1}{2}\hat{\mathbf{P}}'^{\dagger}(\boldsymbol{\sigma}^{\mathrm{T}}\mathbf{G}''^{-1}\boldsymbol{\sigma})|_{\text{eq}}\hat{\mathbf{P}}' \tag{10}$$

Remember that '$|_0$' means that only the inactive coordinates are fixed, whereas '$|_{\text{eq}}$' implies that all coordinates are fixed. The matrix elements of $(-\boldsymbol{\sigma}^{\mathrm{T}}\mathbf{G}''^{-1}\boldsymbol{\sigma})|_{\text{eq}}$ are thus constant.

In Ref. [26], a code, called TNUM, for numerically evaluating all matrix elements appearing in the exact and constrained kinetic energy operator has been presented. In this paper, we propose to combine the polyspherical formalism [22] with the numerical approach of TNUM to derive constrained kinetic energy operators which could be very easily implemented in MCTDH. It should be emphasized that this novel approach could lead to numerous applications. TNUM can be used for several set of coordinates, e.g. polyspherical, z-matrix, Cartesian and coordinate transformations. The constrained operators are derived using the formulation of Ref. [22], i.e. this code numerically provides the matrix elements G appearing in the operators without constraints as well as in the main terms in the constrained operators but also the matrix appearing in the correction, i.e. $(-\boldsymbol{\sigma}^{\mathrm{T}}\mathbf{G}''^{-1}\boldsymbol{\sigma})|_0$ in Eq. (9). Moreover, TNUM also provides the extra-potential term aforementioned. In this paper, we have used TNUM for two purposes: (i) to check that all the matrix elements in G'' were correct (simply but checking that Eq. (11) and TNUM provide the same values as the analytically derived G-matrix for different points on the grid), and (ii) to calculate the correction.

To conclude, Eq. (4) provides the main term analytically in a sum of monomode operators which is the form perfectly adapted to MCTDH and TNUM provides the main part of the correction in a form which is also straightforward to implement. For C_2H_4, when using a Cartesian elementary volume element $\mathrm{d}\tau = \mathrm{d}R_3\mathrm{d}R_4\mathrm{d}R_5\mathrm{d}\theta_1\mathrm{d}\theta_2\mathrm{d}\theta_2\mathrm{d}\varphi_3$, the main term reads

$$\begin{aligned}
2\hat{T}_{\text{main}} = &-\frac{1}{\mu}\frac{\partial^2}{\partial R_1^2} - \frac{1}{\mu}\frac{\partial^2}{\partial R_2^2} - \frac{2}{m_c}\frac{\partial^2}{\partial R_5^2} + \frac{2\cos\theta_1}{m_c}\frac{\partial}{\partial R_1}\frac{\partial}{\partial R_5} \\
&+ \frac{2\cos\theta_2}{m_c}\frac{\partial}{\partial R_2}\frac{\partial}{\partial R_5} + \frac{2\cos\theta_1}{m_c R_1 R_5} + \frac{2\cos\theta_2}{m_c R_2 R_5} - \frac{\partial}{\partial\theta_1} \\
&\times \frac{\sin\theta_1}{m_c R_5}\frac{\partial}{\partial R_1} - \frac{\partial}{\partial R_1}\frac{\sin\theta_1}{m_c R_5}\frac{\partial}{\partial\theta_1} - \frac{\partial}{\partial\theta_2}\frac{\sin\theta_2}{m_c R_5} \\
&\times \frac{\partial}{\partial R_2} - \frac{\partial}{\partial R_2}\frac{\sin\theta_2}{m_c R_5}\frac{\partial}{\partial\theta_2} + \frac{\partial}{\partial\theta_1}\frac{\sin\theta_2\cos\varphi_3}{m_c R_5} \\
&\times \frac{\partial}{\partial R_2} + \frac{\partial}{\partial R_2}\frac{\sin\theta_2\cos\varphi_3}{m_c R_5}\frac{\partial}{\partial\theta_1} + \frac{\partial}{\partial\theta_2} \\
&\times \frac{\sin\theta_1\cos\varphi_3}{m_c R_5}\frac{\partial}{\partial R_1} + \frac{\partial}{\partial R_1}\frac{\sin\theta_1\cos\varphi_3}{m_c R_5}\frac{\partial}{\partial\theta_2} \\
&- \frac{\partial}{\partial\theta_1}\frac{\sin\theta_1}{m_c R_1}\frac{\partial}{\partial R_5} - \frac{\partial}{\partial R_5}\frac{\sin\theta_1}{m_c R_1}\frac{\partial}{\partial\theta_1} - \frac{\partial}{\partial\theta_2}\frac{\sin\theta_2}{m_c R_2} \\
&\times \frac{\partial}{\partial R_5} - \frac{\partial}{\partial R_5}\frac{\sin\theta_2}{m_c R_2}\frac{\partial}{\partial\theta_2} \\
&- \frac{\partial}{\partial\theta_1}\left(\frac{2}{m_c R_5^2} + \frac{1}{\mu R_1^2} + \frac{2\cos\theta_1}{m_c R_1 R_5}\right)\frac{\partial}{\partial\theta_1} \\
&- \frac{\partial}{\partial\theta_2}\left(\frac{2}{m_c R_5^2} + \frac{1}{\mu R_2^2} + \frac{2\cos\theta_2}{m_c R_2 R_5}\right)\frac{\partial}{\partial\theta_2} \\
&+ \frac{\partial}{\partial\theta_1}\left(\frac{\cos\theta_1\cos\varphi_3}{m_c R_1 R_5} + \frac{\cos\theta_2\cos\varphi_3}{m_c R_2 R_5} + \frac{2\cos\varphi_3}{m_c R_5^2}\right)\frac{\partial}{\partial\theta_2} \\
&+ \frac{\partial}{\partial\theta_2}\left(\frac{\cos\theta_1\cos\varphi_3}{m_c R_1 R_5} + \frac{\cos\theta_2\cos\varphi_3}{m_c R_2 R_5} + \frac{2\cos\varphi_3}{m_c R_5^2}\right)\frac{\partial}{\partial\theta_1} \\
&- \frac{\partial}{\partial\varphi_3}\left(\frac{2}{m_h R_3^2} + \frac{2}{m_h R_4^2}\right)\frac{\partial}{\partial\varphi_3}
\end{aligned} \tag{11}$$

where $\mu = \left(\frac{1}{m_c} + \frac{1}{2m_h}\right)^{-1}$.

The (approximate) correction terms, Eq. (10), are provided by TNUM

$$\begin{aligned}
T_{\text{cor}'} = &\ 0.0000019889\frac{\partial^2}{\partial R_5^2} - 0.0000138299\frac{\partial}{\partial R_2}\frac{\partial}{\partial R_5} \\
&- 0.0000138299\frac{\partial}{\partial R_1}\frac{\partial}{\partial R_5} + 0.0000480826\frac{\partial^2}{\partial\theta_2^2} \\
&+ 0.0000480826\frac{\partial^2}{\partial\theta_1^2}
\end{aligned} \tag{12}$$

where atomic units are assumed.

It should be noted that there is an additional extra-potential term originating from the Jacobian of the constraint. In this work, we have neglected this term and checked (with the aid of TNUM) that this extra-potential is singularity free, i.e. does not diverge at $\theta_1 = 0$ or θ_2=0.

For the sake of completeness, we specify the coordinate ranges:

$$\begin{aligned} &0 \leqslant R_i \leqslant +\infty \\ &-\pi \leqslant \theta_i < \pi \\ &0 \leqslant \varphi_3 < 2\pi \end{aligned}$$

Note that the two θ-angles vary over the full circle rather then the half circle. This unusual range is adopted because the corresponding azimuthal angles $\varphi_{1,2}$ are constraint.

Finally, the relation between the polyspherical coordinates and the six degrees of freedom used in Ref. [12] is given by

$$\begin{aligned} r &= R_5 \\ \vartheta_r &= \theta_2 \\ \vartheta_l &= \theta_1 \\ \alpha_r &= 2\arccos(R_2/R_{\mathrm{CH}}) \\ \alpha_l &= 2\arccos(R_1/R_{\mathrm{CH}}) \\ \varphi &= \varphi_3 \end{aligned} \tag{13}$$

where R_{CH} denotes the C–H equilibrium distance. We have also checked that the first kinetic energy operator, Eq. (3), can be extracted from Eq. (11). This can be done by setting μ equal to $2m_h$ and neglecting all terms which include $\left(\frac{1}{m_c}\right)$ except the term $\left(\frac{\partial^2}{\partial R_5^2}\right)$. After erasing all these terms and transforming the coordinates according to Eqs. (13), (11) turns into Eq. (3).

2.4. Propagation algorithm

The wave-packet propagations reported in this article are performed with the Heidelberg MCTDH package [14]. Multi-configuration time-dependent Hartree (MCTDH) [14,27–29] is a general algorithm for solving the time-dependent Schrödinger Equation. In the MCTDH framework the wavefunction is expanded in a sum of Hartree products. These products consist of so called single particle functions (SPF) that depend on time and on one degree of freedom:

$$\Psi(Q_i,\ldots,Q_f,t) = \sum_{j_1=1}^{N_1}\cdots\sum_{j_f=1}^{N_f}\sum_{s} A_{j_1,\ldots,j_f,s}(t)\prod_{\kappa=1}^{f}\varphi_{j_\kappa}^{(\kappa)}(Q_\kappa,t)|s> \tag{14}$$

Here the $\varphi_{j_\kappa}^{(\kappa)}(Q_\kappa,t)$ are the SPFs and the $A_{j_1,\ldots,j_f i,s}(t)$ are the expansion coefficients. The index s runs over the electronic states and $|s>$ denotes a (diabatic) state function. Note that both, SPFs and coefficients, depend on time. The equations of motion are derived with the Dirac-Frenkel variational principle. The SPFs are expanded in a (time-independent) primitive basis. For technical reasons a discrete variable representation (DVR) [30,31] is mostly used. There are N_κ grid points (or primitive basis functions) for the κth degree of freedom (DOF). The DVR's used for the different degrees of freedom are listed in Table 2.

Within this framework the ethene molecule has already been investigated [12]. In the Heidelberg MCTDH package [14] two useful features are additionally implemented

- Multi set formalism. The different electronic states are treated by introducing individual sets of single particle functions for each of the electronic states. This treatment of the electronic states is usually more efficient than the single set formalism discussed above.
- Mode combination. A single particle function can depend on more than one degree of freedom. This complicates the propagation of the now multidimensional single particle functions, but reduces the size of the coefficient vector (A-vector), because some of the correlation is now treated at the SPF level. Mode combination can considerably reduce the numerical effort. (Compare e.g. with chapter 9.4 Table 5 of Ref. [14]).

The MCTDH wavefunction is expanded in the following way for the first KEO:

$$\begin{aligned} &\Psi(r,\varphi,\vartheta_r,\alpha_r,\vartheta_l,\alpha_l,t) \\ &\quad= \sum_{s=0}^{2}\sum_{j_1=1}^{n_{1,s}}\sum_{j_2=1}^{n_{2,s}}\sum_{j_3=1}^{n_{3,s}}\sum_{j_4=1}^{n_{4,s}} A_{j_1,\ldots,j_4}^{(s)}(t)\varphi_{j_1}^{(1,s)}(r,t)\varphi_{j_2}^{(2,s)}(\varphi,t) \\ &\qquad\times \varphi_{j_3}^{(3,s)}(\vartheta_r,\alpha_r,t)\varphi_{j_4}^{(4,s)}(\vartheta_l,\alpha_l,t)|s> \end{aligned} \tag{15}$$

and similarlyand similarly

$$\begin{aligned} &\Psi(R_5,\varphi_3,\theta_1,R_1,\theta_2,R_2,t) \\ &\quad= \sum_{s=0}^{2}\sum_{j_1=1}^{n_{1,s}}\sum_{j_2=1}^{n_{2,s}}\sum_{j_3=1}^{n_{3,s}}\sum_{j_4=1}^{n_{4,s}} A_{j_1,\ldots,j_4}^{(s)}(t)\varphi_{j_1}^{(1,s)}(R_5,t)\varphi_{j_2}^{(2,s)}(\varphi_3,t) \\ &\qquad\times \varphi_{j_3}^{(3,s)}(\theta_1,R_1,t)\varphi_{j_4}^{(4,s)}(\theta_2,R_2,t)|s> \end{aligned} \tag{16}$$

for the second KEO. The number of single particle functions for the different modes, diabatic electronic states and KEOs are listed in Table 3.

There are only two sensible mode-combination schemes. As the r – and φ – grids are rather large, they should be left uncombined. Meaningful combinations are hence (α_r, α_l), (ϑ_r, ϑ_l), or (α_r,ϑ_r), (α_l,ϑ_l). The latter combination scheme was chosen to arrive at equally sized combined grids.

Table 2
DVR type and size for the various degrees of freedom

First KEO				Second KEO			
DOF	N	Range	DVR	DOF	N	Range	DVR
r	60	[1.61; 4.22]	HO	R_5	60	[1.61; 4.22]	HO
φ	128	[−180°; 180°]	FFT	φ_3	128	[−180°; 180°]	FFT
α_r	20	[54°; 169°]	sin	R_1	20	[0.19; 1.82]	HO
α_l	20	[54°; 169°]	sin	R_2	20	[0.19; 1.82]	HO
ϑ_r	32	[−80°; 80°]	sin	θ_1	32	[−80°; 80°]	sin
ϑ_l	32	[−80°; 80°]	sin	θ_2	32	[−80°; 80°]	sin

Table 3
Single particle function basis sets for the first and second KEO and all three different propagations. Furthermore, memory requirements and computation times are displayed

State		Set 1			Set 2			Set 3		
First KEO	Second KEO	N	Z	V	N	Z	V	N	Z	V
r	R_5	10	10	12	12	12	15	16	16	18
φ	φ_3	40	40	40	40	40	40	40	40	40
(α_l, ϑ_l)	(R_1, θ_1)	12	12	14	14	14	18	20	20	30
(α_r, ϑ_r)	(R_2,θ_2)	12	12	14	14	14	18	20	20	30
SPF basis set size		209,280			382,560			1,160,000		
Memory		140 MB			190 MB			400 MB		
CPU-time first/second KEO		40 h/74 h			60 h/114 h			182 h/367 h		

2.5. Propagation of the wave-packet

An investigation of a photo-excitation process starts with preparing an initial wave-packet. The initial wavefunction was prepared by relaxing (propagating in imaginary time) a Gaussian wave-packet placed initially on the diabatic N state (ground state). For the relaxation the complete Hamiltonian was used, i.e. all three electronic states were included. The converged ground state wavefunction has some small occupations on the V and Z states. To model the photo-excitation process the ground state wavefunction was projected onto the electronic N state (i.e. the small V and Z state populations were removed), renormalized, and then moved vertically to the V state (Condon approximation). This initial wave-packet was propagated for 250 fs with different sets of single particle functions (see Table 3).

3. Calculation methods for the adiabatic state populations

The calculation of the adiabatic state populations is easy when the adiabatic representation is used. Then the population of the different adiabatic electronic states are the expectation values of the projection matrices for the corresponding state.

$$p_i = \langle \underline{\Psi}^{\mathrm{ad}} | \underline{\underline{\widetilde{P}}}^{(i)} | \underline{\Psi}^{\mathrm{ad}} \rangle. \tag{17}$$

Where $\underline{\Psi}^{\mathrm{ad}}$ denotes the nuclear wavefunction in adiabatic representation and $(\underline{\underline{\widetilde{P}}}^{(i)})_{kl} = \delta_{kl}\delta_{ki}$ the projection matrix which projects onto the i-th state. But in general the propagation is performed in the diabatic picture. Therefore the diabatic to adiabatic transformation matrix is needed, which is just the eigenvector matrix of the diabatic potential $\underline{\underline{W}}$

$$\underline{\underline{W}} = \underline{\underline{U}}\,\underline{\underline{V}}\,\underline{\underline{U}}^{\dagger} \tag{18}$$

where $\underline{\underline{V}}$ is the (diagonal) adiabatic potential matrix. Note, that $\underline{\underline{U}}$ depends on the nuclei coordinates. The adiabatic wavefunction can be expressed as

$$|\underline{\Psi}^{\mathrm{ad}}\rangle = \underline{\underline{U}}^{\dagger} |\underline{\Psi}^{\mathrm{dia}}\rangle \tag{19}$$

Inserting this into Eq. (17) leads to:

$$\begin{aligned} p_i &= \langle \underline{\Psi}^{\mathrm{ad}} | \underline{\underline{\widetilde{P}}}^{(i)} | \underline{\Psi}^{\mathrm{ad}} \rangle = \langle \underline{\Psi}^{\mathrm{dia}} | \underline{\underline{U}}\,\underline{\underline{\widetilde{P}}}^{(i)}\,\underline{\underline{U}}^{\dagger} | \underline{\Psi}^{\mathrm{dia}} \rangle \\ &= \langle \underline{\Psi}^{\mathrm{dia}} | \underline{\underline{P}}^{(i)} | \underline{\Psi}^{\mathrm{dia}} \rangle \end{aligned} \tag{20}$$

where $\underline{\underline{P}}^{(i)} = \underline{\underline{U}}\,\underline{\underline{\widetilde{P}}}^{(i)}\,\underline{\underline{U}}^{\dagger}$ is the projection matrix onto the ith adiabatic state in diabatic representation. Eq. (20) offers two ways to calculate the adiabatic state populations:

- Calculating the adiabatic wavefunction by transforming the wavefunction $|\underline{\Psi}^{\mathrm{ad}}\rangle = \underline{\underline{U}}^{\dagger} |\underline{\Psi}^{\mathrm{dia}}\rangle$ and then using the projector $\underline{\underline{\widetilde{P}}}^{(i)}$.
- Calculating the projection matrix $\underline{\underline{P}}^{(i)}$ for the diabatic picture and then evaluating the expectation value $\langle \underline{\Psi}^{\mathrm{dia}} | \underline{\underline{P}}^{(i)} | \underline{\Psi}^{\mathrm{dia}} \rangle$.

Both ways have been implemented in the Heidelberg MCTDH package. The first algorithm is simple to use and works well for small systems. The second algorithm, however, is more powerful and more efficient and has been used for the calculation of the adiabatic state populations of ethene. It is called *adproj* algorithm and consists of several steps that are described in the following.

First the *adproj* program calculates the matrix elements of the projection matrix in the diabatic basis for each electronic state. These matrix elements are complicated functions of the internal coordinates. The matrix elements are then fitted to product representation with the so called *potfit* algorithm [32,33,14]. *Potfit* is an algorithm that is used to transform multidimensional functions (usually potentials) to product representation. The algorithm is approximate in general but it becomes numerically exact if the maximum number of expansion terms is used. Usually a much smaller number of expansion terms is sufficient to obtain an adequate accuracy for the fitted functions. After the matrix elements of the projector are potfitted, MCTDH operators are build. As the last step the expectation values of the projection operators are calculated for every time-step. Because of the product structure of the projector the evaluation of the expectation values is quite efficient, albeit the most time-consuming step of the procedure.

4. Calculation of the adiabatic state populations of ethene

In the following the calculation of the adiabatic state populations of ethene will be described. As already mentioned the *adproj* algorithm has been used. But it turns out that in the case of C_2H_4 it was not possible to use *adproj* straightforwardly because of the too large product-grid size. To tackle this problem the following consideration is made.

For an accurate description of a wavefunction the grid must be densely spaced because a wavefunction is a strongly oscillating function of the spatial degrees of freedom. But this is not true for the potential energy surfaces. These are usually much smoother compared to the wavefunction. Hence for a proper description of potential functions or projection operator matrix elements a coarser grid suffices. Following this idea the number of grid points was reduced by a common factor for each degree of freedom, resulting in a smaller primitive grid for the *adproj* and *potfit* runs. After the *potfit* step the (electronic) matrix elements of the projectors, which are potential like functions, have been interpolated to the original number of grid points. The reduction of the grid size was tested and compared for different coarsening factors. In Fig. 2 the results for the different tests are shown. The factors 1/4, 1/2 and 3/4, applied to each degree of freedom, have been used. The difference between these calculations is in the order of 10^{-5} for the whole propagation time (All lines are also shown in the inset of Fig. 2 but are not distinguishable on this scale.). The error introduced by the coarsening of the grid is thus very small. For the following calculations of projection operators a coarsening factor of 1/2 has been used.

As already discussed the convergence of the operator in the *potfit* step must be guaranteed. In Fig. 3 the adiabatic state populations for the ground state are displayed. These calculations have been done with different numbers of natpot terms. As one can see the small projection operator produces inaccurate results for short propagation times (negative state populations have no physical meaning) but reveals the main features for large propagation times and is just one percent off the better converged results (Again, all lines are shown in the inset of Fig. 3 but are indistinguishable on this scale). The *potfit* step hence introduces negligible errors if a sufficiently large number of natpot terms (e.g. 6000 in this case) is used. We finally comment on the numerical effort of the *adproj* method. The evaluation of the expectation value of the projection takes by far most of the effort, the *adproj* and *potfit* steps are much faster. This is because the expectation value has to be computed 3×250 times for each run (for three states and 250 time-steps). The total effort for computing the adiabatic state populations is about twice the effort for the propagation.

5. Computational results

5.1. Convergence quality

To check the convergence of the calculations with respect to the numbers of SPFs, we have run three propagations with increasing numbers of SPFs (see Table 3).

A useful indicator for the quality of the wave-packet propagation is the population of the least populated natural orbital. In earlier calculations it turned out that a population of less than 10^{-2} (better 10^{-3}) for the least populated natural orbital indicates a reasonable converged calculation. In Tables 4 and 5 the maxima over time for the population of the least populated natural orbitals are given for the different single particle function sets and for the old and new KEO calculations.

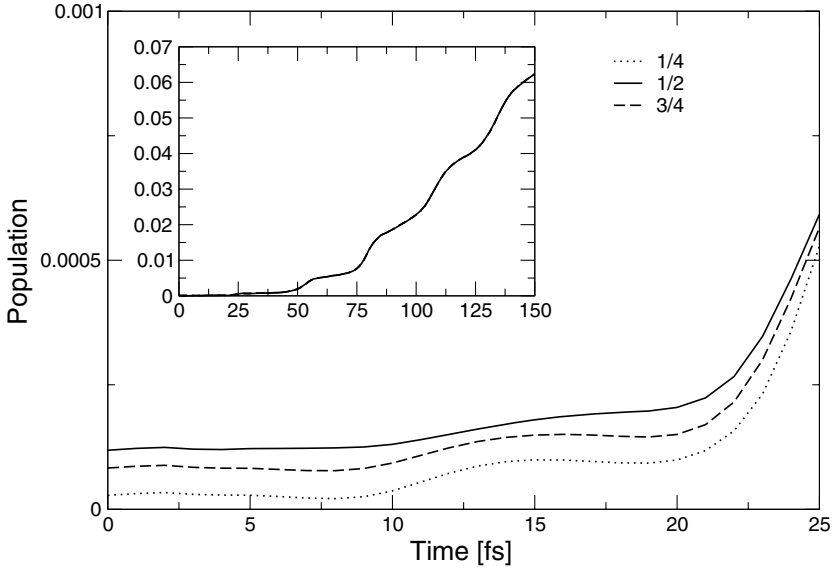

Fig. 2. Convergence of the projection operator for the adiabatic ground state for coarsened grids. Note the ordinate scale! The inset shows all lines up to 150 fs.

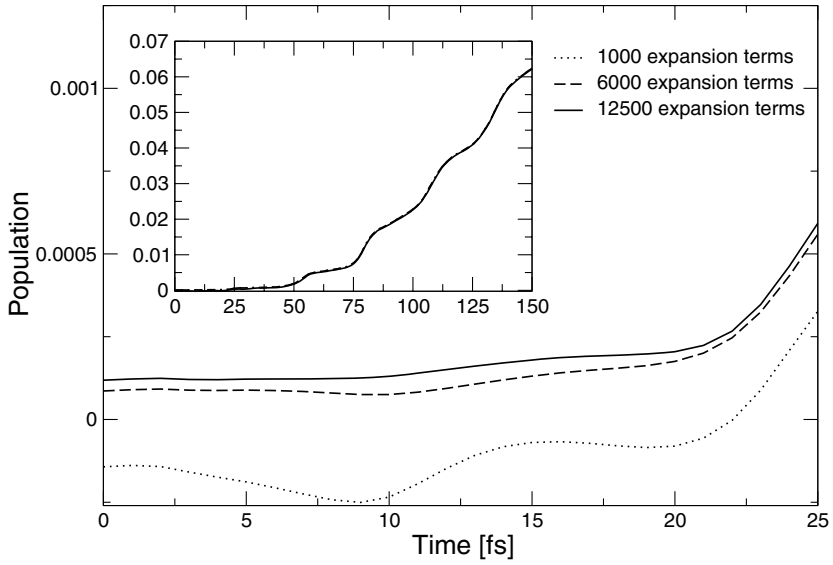

Fig. 3. Convergence of the projection operator for the adiabatic ground state, different numbers of natpot terms have been used. Note the ordinate scale! The inset shows all lines up to 150 fs. No differences are visible on the larger scale.

Table 4
Highest population (over all times) of the least occupied natural orbital for the first KEO

Mode	N	Z	V
SPF basis set 1			
r	1.15×10^{-2}	1.17×10^{-2}	1.95×10^{-2}
φ	6.72×10^{-4}	6.82×10^{-4}	7.72×10^{-4}
$\alpha_r\times\vartheta_r$	1.04×10^{-2}	9.94×10^{-3}	1.94×10^{-2}
$\alpha_l\times\vartheta_l$	1.02×10^{-2}	1.03×10^{-2}	1.98×10^{-2}
SPF basis set 2			
r	7.20×10^{-3}	7.16×10^{-3}	4.54×10^{-3}
φ	4.74×10^{-4}	4.50×10^{-4}	5.20×10^{-4}
$\alpha_r\times\vartheta_r$	8.10×10^{-3}	8.44×10^{-3}	1.24×10^{-2}
$\alpha_l\times\vartheta_l$	8.22×10^{-3}	8.13×10^{-3}	1.15×10^{-2}
SPF basis set 3			
r	2.50×10^{-3}	2.38×10^{-3}	8.36×10^{-4}
φ	3.27×10^{-4}	3.26×10^{-4}	3.74×10^{-4}
$\alpha_r\times\vartheta_r$	5.00×10^{-3}	5.03×10^{-3}	4.03×10^{-3}
$\alpha_l\times\vartheta_l$	5.03×10^{-3}	4.98×10^{-3}	4.19×10^{-3}

Table 5
Highest population (over all times) of the least occupied natural orbital for the second KEO

Mode	N	Z	V
SPF basis set 1			
R_5	9.19×10^{-3}	9.44×10^{-3}	1.13×10^{-2}
φ_3	5.21×10^{-4}	5.12×10^{-4}	5.41×10^{-4}
$R_1\times\theta_1$	1.15×10^{-2}	1.14×10^{-2}	2.56×10^{-2}
$R_2\times\theta_2$	1.15×10^{-2}	1.16×10^{-3}	2.40×10^{-2}
SPF basis set 2			
R_5	6.94×10^{-3}	6.89×10^{-3}	4.15×10^{-3}
φ_3	4.23×10^{-4}	4.35×10^{-4}	4.93×10^{-4}
$R_1\times\theta_1$	9.75×10^{-3}	9.71×10^{-3}	1.54×10^{-2}
$R_2\times\theta_2$	9.69×10^{-3}	9.99×10^{-3}	1.55×10^{-2}
SPF basis set 3			
R_5	3.50×10^{-3}	3.52×10^{-3}	1.32×10^{-4}
φ_3	3.61×10^{-4}	3.64×10^{-4}	3.93×10^{-4}
$R_1\times\theta_1$	5.91×10^{-3}	6.04×10^{-3}	6.84×10^{-3}
$R_2\times\theta_2$	5.91×10^{-3}	5.91×10^{-3}	6.95×10^{-3}

A more stringent convergence check is provided by comparing observables calculated with different basis sets. The observables of interest here are the adiabatic state populations. The most sensitive one is the adiabatic ground state population because its value is one order of magnitude smaller than the populations of the two other states. In Fig. 4 the adiabatic ground state populations for the three basis sets are displayed for the second KEO calculations. The populations for the basis sets 2 and 3 lie close together but the population for the smallest basis set becomes too small after 100 fs. The ground state populations evaluated with the first KEO are not displayed. They show a similar pattern but lie closer together over the whole interval of 250 fs. This means that it is easier to converge the calculations with the first KEO than those with the second. This can also be seen if one compares the populations of the highest natural orbitals. In the case of the first KEO their values are always smaller than those of the second KEO calculations. The following investigations will refer to the propagations with the basis sets 2 and 3.

5.2. Autocorrelation function and absorption spectrum

The Fig. 5 shows the absolute value ($|c(t)|$) of the autocorrelation function for the old and new KEO calculations. It is possible to calculate the autocorrelation function for twice the propagation time because the initial wavefunction is real and the following equation can be used for the calculation of the autocorrelation function:

$$c(t) = < \Psi^*(t/2)|\Psi(t/2) > \tag{21}$$

The value of $|c(t)|$ decays rapidly to a value of about 0.2% in both cases. After about 50 fs a major recurrence takes place and the $|c(t)|$ rises to a value of about 20%. After this

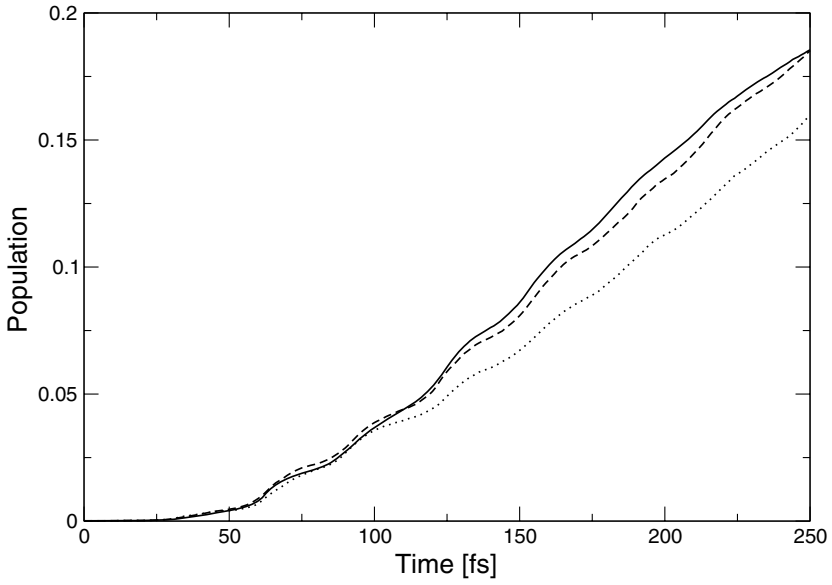

Fig. 4. Adiabatic ground state population for the second KEO. The dotted line is for the SPF-basis set 1, the dashed line for set 2 and the solid line for set 3.

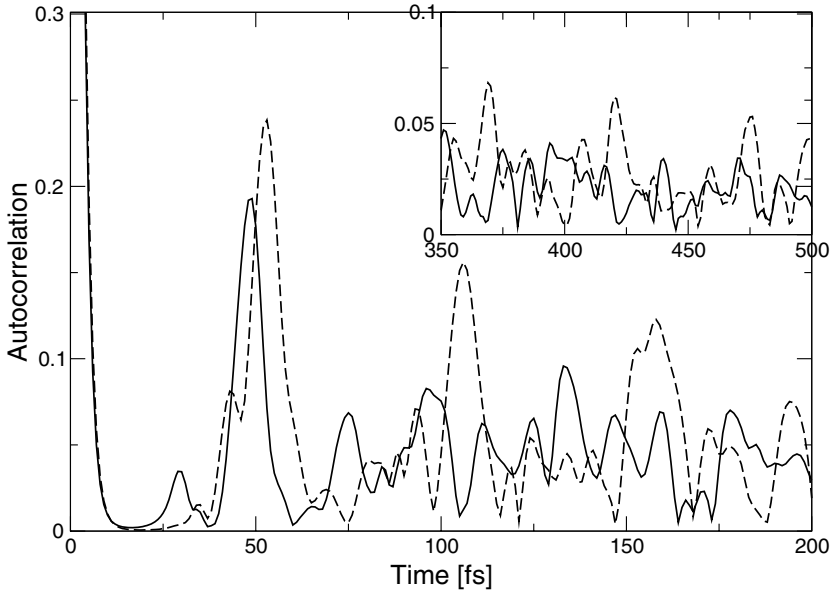

Fig. 5. Autocorrelation function for the first (solid line) and second (dashed line) KEO.

the autocorrelation function computed with the first KEO becomes more diffuse whereas the one of the second KEO shows further recurrences at about 100 fs and 150 fs. For large propagation times both autocorrelation functions show a rather diffuse pattern, but the one of the second KEO is still more structured (see inset). If the autocorrelation function is compared with the one of Ref. [12], one should note that there $|c(t)|^2$ is plotted rather than $|c(t)|$.

The corresponding spectra, displayed in Fig. 6, can be obtained by a Fourier transformation of the autocorrelation function. To reduce the effects of the Gibbs phenomenon in the Fourier transformation usually a damping function is applied. In the present case a squared cosine was used. Additionally for both kinetic energy operators the spectrum has been calculated again by additionally multiplying the autocorrelation function with the damping function $\exp(-t^2/t_{\mathrm{damp}}^2)$ (t_{damp}=100 fs), to make the spectra comparable to those in Ref. [12]. Furthermore, the energy scales of all spectra are, of course, defined with respect to the ground state energy which read $E_0^{\mathrm{first}} = 0.484921$ eV or $E_0^{\mathrm{second}} = 0.511265$ eV, respectively.

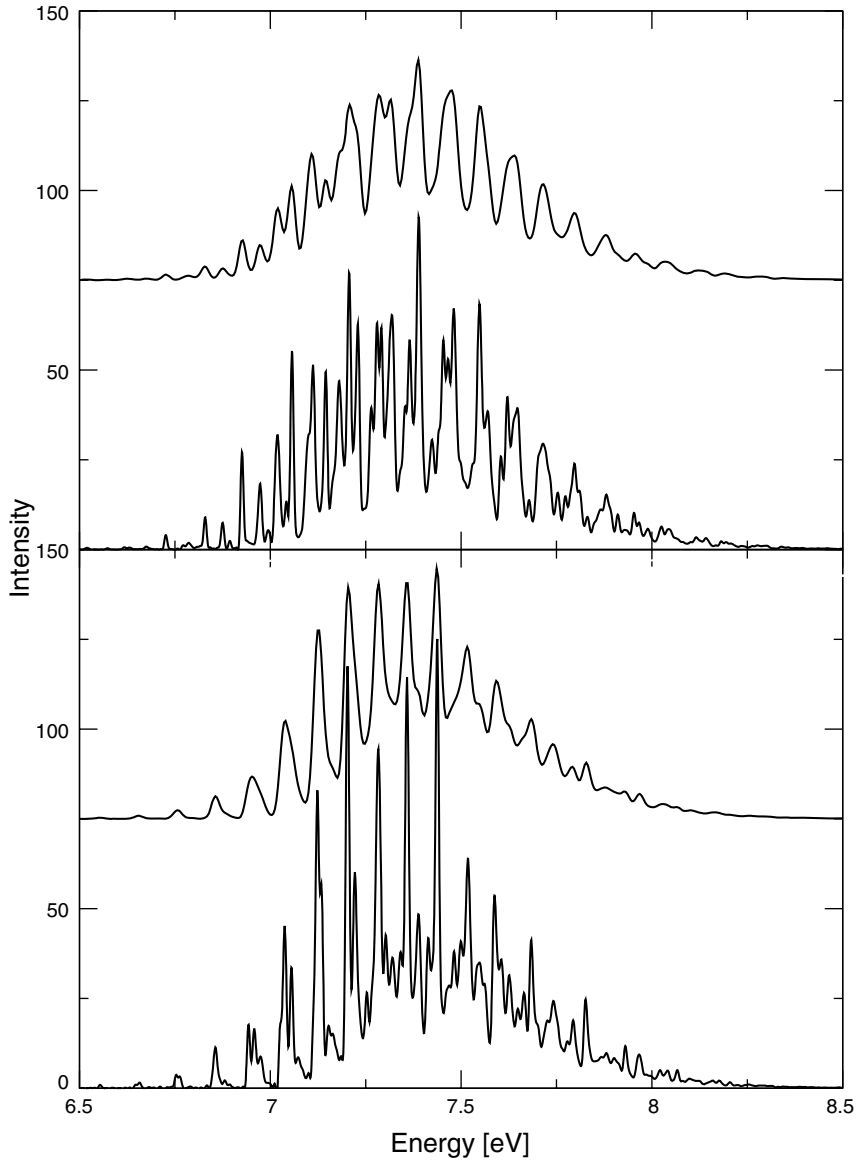

Fig. 6. Absorption spectrum for $\pi \rightarrow \pi^*$ excitation. The upper part shows the spectra obtained with the first KEO and the lower part the one with the second KEO. Low resolution spectra, obtained by convolution with a Gaussian (see text) are also shown. These are shifted vertically to increase visibility.

The spectra for the first and second KEO show clear differences. In the first KEO case the peak structure is less regular on the low-energy side than on the high-energy side. This is in contrast to the second KEO case, where the spectrum is much more structured in the low-energy range compared to the high-energy range. Furthermore the second spectrum itself is less diffuse compared to the first one. This is caused by the stronger recurrences in the autocorrelation function of the second KEO case.

A further difference is the mean peak spacing around the maximum. In the case of the first KEO it is about 680 cm^{-1} compared to 650 cm^{-1} for the second KEO. This is lower than the experimentally observed value of 800 cm^{-1} [34]. However, the spectrum obtained with the second KEO shows a mean peak spacing of about 805 cm^{-1} in the lower energy range of 6.5–7.0 eV. This is precisely the energy range where the mean peak spacing of 800 cm^{-1} is found in Ref. [34].

5.3. Adiabatic and diabatic state populations

The main focus of the present work is on the calculation of the diabatic and adiabatic state populations of the $\pi \rightarrow \pi^*$-excited ethene molecule. The Figs. 7 and 8 show the diabatic state populations for the whole propagation time for the first and second kinetic energy operator. In the case of the first KEO the population of the diabatic V state stays close to 1 for the first 10 fs, after this the population drops and an oscillatory behavior occurs with an oscillation period of about 25 fs. This structure becomes more and more washed out and finally disappears after 200 fs revealing the underlying process of a steady decrease

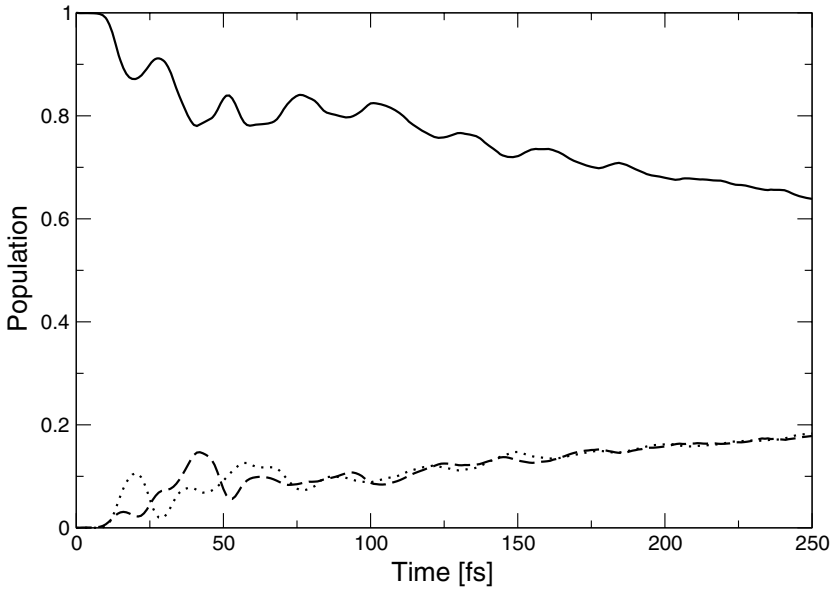

Fig. 7. Diabatic state populations computed with the first KEO. (N state: dashed line; V state: solid line; Z state: dotted line).

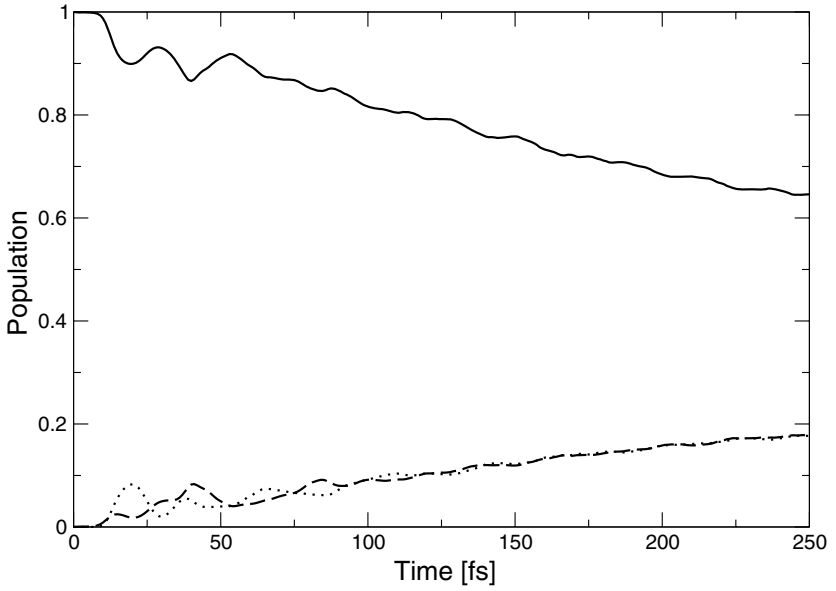

Fig. 8. Diabatic state populations computed with the second KEO. (N state: dashed line; V state: solid line; Z state: dotted line).

of the V state population. Calculations using the second KEO show a similar behaviour, but now the oscillations are less pronounced and the almost linear drop of the population already occurs after 75 fs. After 250 fs the V state population is about 0.65 for both KEOs.

The two other diabatic states, the N and the Z state, show almost the same behavior. Both start with a population of zero and they become populated over the propagation time. For the first 100 fs the population of the two states evolves oscillatory with unstructured rises and drops. Afterwards they come close to each other and rise almost linearly to a value of about 0.18 after 250 fs. Both sets of diabatic populations, calculated with the first and second KEO, respectively, show a similar behavior, but in the case of the second KEO the rises and drops of the N and Z state populations within the first 100 fs are less pronounced compared to those in the first KEO case.

In the Fig. 9 the adiabatic populations for the excited states S_1 and S_2 are displayed. Whereas in Fig. 10 the adiabatic ground state (S_0) is shown for both kinetic energy operators. A comparison with the Figs. 7 and 8 shows that the population of the adiabatic S_1 state and the diabatic V state are very similar. The adiabatic S_0 and the S_2 states, however, are obviously mixtures of the diabatic N and Z states.

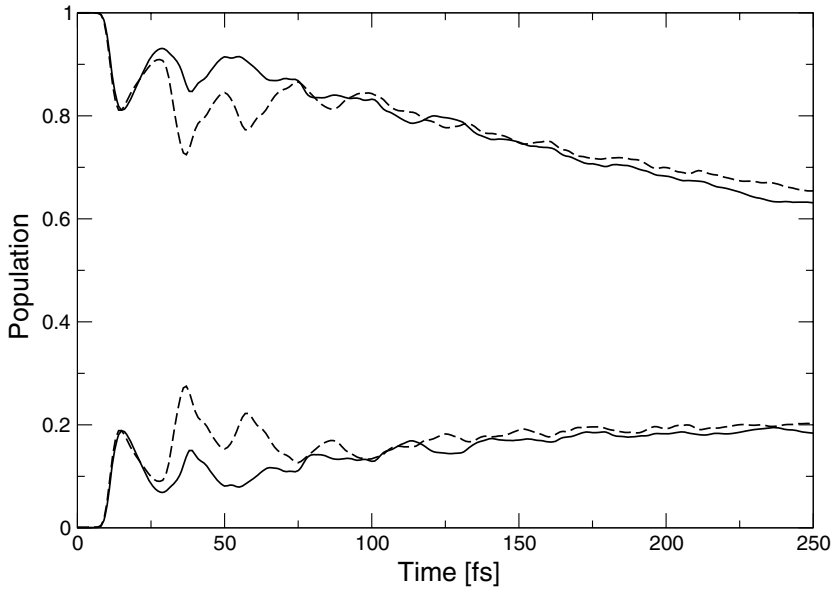

Fig. 9. Adiabatic state populations computed with the first and second KEO, respectively. The upper lines are the populations of the S_1 state and the lower lines are the populations for the S_2 state (first KEO: dashed lines, second KEO: solid lines). The population of the adiabatic ground state S_0 is not displayed here. See next figure.

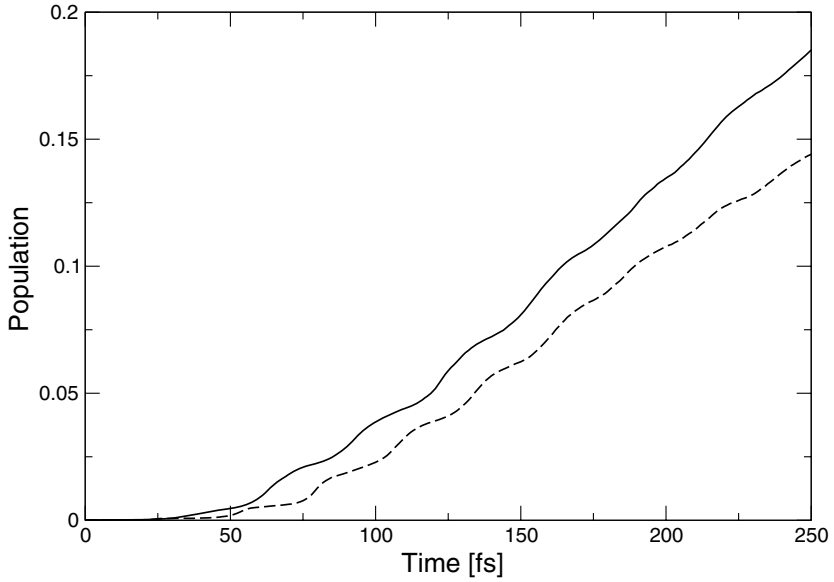

Fig. 10. Adiabatic ground state (S_0) populations computed with the first (dashed line) and second (solid line) KEO, respectively.

The population of the S_2 state behaves like the S_1 state population mirrored at the centerline of the figure. This is due to the fact that the S_0 state population is very low for the first part of the propagation time. For higher propagation times ($\geqslant 50$ fs) the population of the S_2 state can be described as above but with an increasing offset (the S_0 state population increases almost linearly). At the end of the propagation time the S_2 and S_1 state populations are almost equal for both kinetic energy operators but a few percent higher for the first kinetic energy. The main difference between the old and new KEO calculations is found in the S_0 state populations. The ground state becomes populated stepwise. Every 50 fs such a step can be found. This structures are washed out for longer propagation times. This is similar in the case of the second KEO but the steps occur at different times compared to the first KEO and they are less pronounced. Furthermore the ground state population rises more strongly in the calculation with the second

KEO. After 250 fs the population reaches 0.185 whereas it is only 0.144 for the first KEO calculation.

The periodic structures in the state populations can be explained as follows. At the beginning of the calculation the wavefunction is localized and when the localized wave-packet comes close to a conical intersection population is transferred between the states. For proceeding propagation time the wave-packet is smeared out and the effect disappears. The fact that the 50 fs structure is less pronounced and faster decaying in the case of the second KEO indicates that this operator provides a more efficient process to diffuse the wave-packet. The topology of the PES and the location of the conical intersections are discussed in detail in Ref. [7].

5.4. Influence of the correction terms for the new KEO

In the derivation of the constrained kinetic energy operator correction terms have been introduced to account for the frozen degrees of freedom. To illustrate the influence of these terms to the numerical results, wave-packet propagations have been performed without these corrections. For these wave-packet propagations the single particle functions SPF-basis set 2 was used. The correction lowers the ground state energy by 39.5 meV, the ground state energies with and without correction read 0.511265 eV and 0.550901 eV, respectively

To further investigate the importance of the corrections, the adiabatic state populations have been computed with and without corrections. These are displayed in Fig. 11. In general the changes introduced by the neglect of the correction terms are minor. Only when turning to the ground state, S_0, population the changes become significant, simply because the ground state population is so small. Here the neglect of the correction modifies the population by about 10%. Hence the influence of the correction terms is clearly visible, but small. This result justifies our approach of treating the corrections approximately when deriving the kinetic energy operator.

6. Conclusion

Following the investigations by Viel et.al. [12] time-dependent wave-packet calculations are performed for the ethene molecule. The six-dimensional potential energy surface derived in Ref. [7] is used together with a kinetic energy operator introduced in Ref. [12]. Additionally a new kinetic operator has been developed that is less approximate, albeit still not exact. The only approximations made are a simplified form of the correction terms and the neglect of an extra-potential term. Wave-packet propagations up to 250 fs are performed for both kinetic energy operators.

The calculations made with the first KEO are in good agreement with those made by Viel et. al. [12]. The present calculations are better converged and show some differences in detail, but the general findings of Ref. [12] are confirmed. The new calculations also significantly extend the propagation time.

The results of the calculations performed with the first KEO are compared with those obtained from propagations which used a newly developed second KEO. The results of the propagations show two main differences: Firstly, the details of the spectra differ essentially. The spectrum received with the first KEO is less structured than the spectrum obtained with the second KEO. As discussed above,

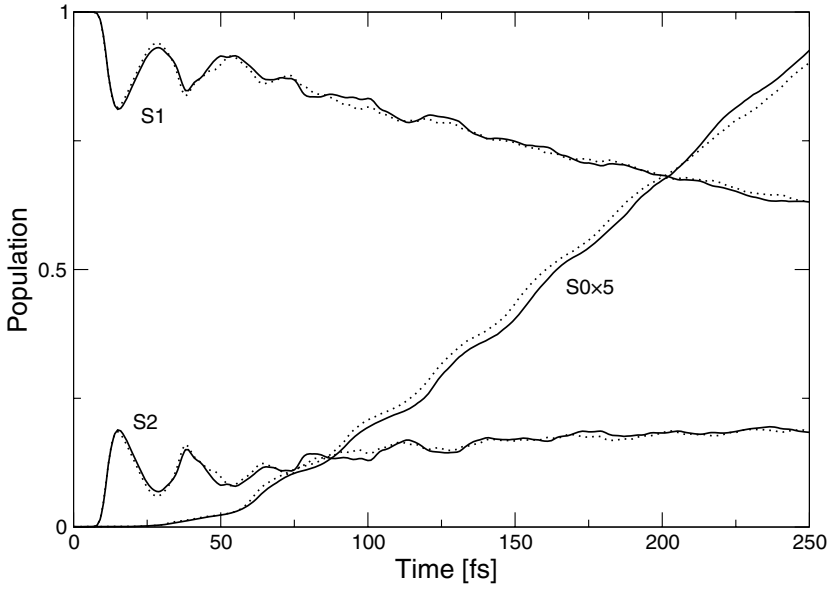

Fig. 11. Adiabatic state populations computed with the second KEO and with (solid line) and without (dotted line) correction terms. The adiabatic ground state population is scaled with a factor of 5.

the second spectrum compares better with experimental data than the first one. Secondly, the adiabatic ground state populations differ. The adiabatic ground state is less populated when using the first KEO. After about 50 fs the population increases to reach 0.144 at 250 fs. The population computed with the second KEO starts to increase earlier. Already after 30 fs the population starts rising and lies always above the population of the first KEO case. At 250 fs it reaches 0.185 what is almost 30% above the result obtained with the first KEO.

Viel et al [12] evaluated the adiabatic populations for the first 50 fs. The present results show that the essential part of the population transfer to the ground state occurs just after this initial period and the transfer is still not finished after 250 fs.

However, the present results are in contradiction to experimental ones [35,36]. An analysis of the experiments yield a transition time to the ground state of 30 ± 15 fs or 20 ± 10 fs, respectively. Moreover, theoretical studies using on-the-fly direct dynamics and incorporating all 12 internal degrees of freedom [10,11] predicted conversion times of about 50 fs. This contradiction indicates that the model potential used is too poor. Fixing all C–H distances to their equilibrium value seems to be a too crude approximation. The decay mechanism of the V state involves two conical intersections, one between V and Z state and one between Z and N state, as described in Ref. [36]. These conical intersections are more easily accessible if the C–H stretches are allowed to adjust accordingly [3,13,36]. As they are frozen, the nonadiabatic transfer is hindered and the resulting radiationless transition rate is much too small.

Last but not least it should be mentioned that in this paper we have derived and applied a new method for computing adiabatic state populations from diabatic MCTDH wave functions.

Acknowledgements

HDM thanks A. Viel for fruitful discussions on the dynamics of ethene and for making the ethene potential available to us. MRB thanks the International Graduiertenkolleg IGK 710 ‘‘Complex processes: Modeling, Simulation and Optimization’’ for a fellowship. Financial support by the Deutsche Forschungsgemeinschaft is gratefully acknowledged.

References

[1] R.J. Buenker, V. Bonačić-Koutecký, L. Pogliani, J. Chem. Phys. 73 (1980) 1836.
[2] M. Persico, V. Bonačić-Koutecký, J. Chem. Phys. 76 (1982) 6018.
[3] I. Ohmine, J. Chem. Phys. 83 (1985) 2348.
[4] S. Krebs, R.J. Buenker, J. Chem. Phys. 106 (1997) 7208.
[5] T. Müller, M. Dallos, H. Lischka, J. Chem. Phys. 110 (1999) 7176.
[6] M. Ben-Nun, T.J. Martínez, Chem. Phys. 259 (2000) 237.
[7] R.P. Krawczyk, A. Viel, U. Manthe, W. Domcke, J. Chem. Phys. 119 (2003) 1397.
[8] M. Barbatti, J. Paier, H. Lischka, J. Chem. Phys. 121 (2004) 11614.
[9] J.C. Tully, J. Chem. Phys. 93 (1990) 1061.
[10] M. Ben-Nun, T.J. Martínez, Chem. Phys. Lett. 298 (1998) 57.
[11] G. Granucci, M. Persico, A. Toniolo, J. Chem. Phys. 114 (2001) 10608.
[12] A. Viel, R.P. Krawczyk, U. Manthe, W. Domcke, J. Chem. Phys. 120 (2004) 11000.
[13] M. Barbatti, M. Ruckenbauer, H. Lischka, J. Chem. Phys. 122 (2005) 174307.
[14] M.H. Beck, A. Jäckle, G.A. Worth, H.-D. Meyer, Phys. Rep. 324 (2000) 1.
[15] A. Viel, R.P. Krawczyk, U. Manthe, W. Domcke, Angew. Chem. 42 (2003) 3434.
[16] F. Gatti, C. Iung, M. Menou, Y. Justum, A. Nauts, X. Chapuisat, J. Chem. Phys. 108 (1998) 8804.
[17] F. Gatti, C. Iung, M. Menou, X. Chapuisat, J. Chem. Phys. 108 (1998) 8821.
[18] F. Gatti, J. Chem. Phys. 111 (1999) 7225.
[19] F. Gatti, C. Munoz, C. Iung, J. Chem. Phys. 114 (2001) 8275.
[20] C. Iung, F. Gatti, Int. J. Quant. Chem. 106 (2006) 130.
[21] A. Nauts, X. Chapuisat, Chem. Phys. Lett. 136 (1987) 164.
[22] F. Gatti, Y. Justum, M. Menou, A. Nauts, X. Chapuisat, J. Mol. Spec. 181 (1997) 403.
[23] E. Wilson, J. Decius, P. Cross, Molecular Vibrations, McGraw-Hill, New York, 1955.
[24] J.E. Hadder, J.H. Frederick, J. Chem. Phys. 97 (1992) 3500.
[25] F. Gatti, Chem. Phys. Lett. 373 (2003) 146.
[26] D. Lauvergnat, A. Nauts, J. Chem. Phys. 116 (2002) 8560.
[27] H.-D. Meyer, U. Manthe, L.S. Cederbaum, Chem. Phys. Lett. 165 (1990) 73.
[28] U. Manthe, H.-D. Meyer, L.S. Cederbaum, J. Chem. Phys. 97 (1992) 3199.
[29] H.-D. Meyer, G.A. Worth, Theor. Chem. Acc. 109 (2003) 251.
[30] J.C. Light, I.P. Hamilton, J.V. Lill, J. Chem. Phys. 82 (1985) 1400.
[31] J.C. Light, T. Carrington Jr., Adv. Chem. Phys. 114 (2000) 263.
[32] A. Jäckle, H.-D. Meyer, J. Chem. Phys. 104 (1996) 7974.
[33] A. Jäckle, H.-D. Meyer, J. Chem. Phys. 109 (1998) 3772.
[34] A.J. Merer, R.S. Mulliken, Chem. Rev. 69 (1968) 639.
[35] P. Farmanara, V. Stert, W. Radloff, Chem. Phys. Lett. 288 (2000) 518.
[36] J.M. Mestdagh, J.P. Visticot, M. Elhanine, B. Soep, J. Chem. Phys. 113 (2000) 237.